Donor spectroscopy in $Hg_{1-x}Cd_xTe$ at high magnetic fields

J. B. Choi and H. D. Drew
Joint Program for Advanced Electronic Materials, Department of Physics and Astronomy, University of Maryland, College Park, Maryland 20742-4111 and Laboratory for Physical Science, College Park, Maryland 20470
(Received 14 August 1989; revised manuscript received 18 December 1989)

Far-infrared magnetotransmission studies of n-type $Hg_{1-x}Cd_xTe$ ($0.2<x<0.3$) are reported for temperatures down to 1.5 K and magnetic fields up to 9 T in Voigt and Faraday geometries. Magneto-optical transitions of donor-bound electrons are observed, including the [000]→[001] and $[0\bar{1}0]\rightarrow[0\bar{1}k_z]$ transitions in the Voigt geometry, and the [000]→[110] transition in the Faraday geometry. These identifications are confirmed by the resonance positions, selection rules, and temperature dependence. The experimental observations are consistent with calculations of resonance positions and line shapes based on the hydrogenic donor model including central-cell effects and band nonparabolicity. This work confirms the donor-bound–electronic ground state for n-type $Hg_{1-x}Cd_xTe$.

I. INTRODUCTION

The narrow-band-gap semiconductors n-type $Hg_{1-x}Cd_xTe$ (MCT) and n-type InSb have long been considered as suitable candidates for the study of magnetic-field-induced localization because they can satisfy the Mott criterion for the metal-insulator transition at readily achievable carrier densities and magnetic fields.[1–4] MCT is particularly attractive because the effective Bohr radius can be varied by changing the Cd concentration x so that the critical magnetic field B_c for the transition can be tuned both by varying x and the carrier density. However, sufficiently high-quality samples of MCT have only recently become available. Therefore, unlike InSb, where the condensation of the electrons onto donors at high fields and low temperatures has been well established, the nature of the ground state of n-type MCT has been controversial.

This controversy centers on whether the observed localization corresponds to condensation of the electrons into a periodic electron lattice as predicted by Wigner (driven by the electron-electron interaction) or to the randomly distributed donors (Mott-Anderson transition). Studies based on transport measurements alone have not resolved this controversy because transport measurements are notoriously difficult to interpret and the Mott-localization criterion [$n^{1/3}a^*(B)=0.25$] applies to both cases. Since this issue has remained unresolved, it is important to clearly establish the nature of the ground state in this material. Far-infrared magnetospectroscopy of the impurity-bound electrons, which should settle the issue, has only recently been reported in MCT.[5–7] The study of shallow donor levels is of importance not only because of the more conclusive and direct evidence for the properties of the electronic ground state in high fields and low temperatures, but because it may also lead to a method of identifying the donor impurities through their chemical shifts (i.e., the central-cell effect). Therefore, these studies could lead to the development of higher-quality MCT and improved optical and electronic devices based on this semiconductor alloy.

In this paper we present the results of extensive studies of the far-infrared magneto-optical transitions of donor-bound electrons in MCT. We report on the [000]→[001] impurity transition and the $[0\bar{1}0]\rightarrow[0\bar{1}k_z]$ photoionization transition in the Voigt geometry, which involve only states associated with the lowest Landau level, and the [000]→[110] transition (impurity cyclotron resonance) in the Faraday geometry, in which the final state is a donor state associated with the first-excited Landau level. The magnetic field dependence of the resonance energies, their selection rules, and the temperature dependence of the observed spectra confirm the identifications of these impurity transitions. Their oscillator strengths demonstrate that nearly all of the extrinsic electrons are on donor sites at sufficiently low temperatures. Central-cell effects are included in the analysis of the transitions from the [000] donor ground state. The $[0\bar{1}0]\rightarrow[0\bar{1}k_z]$ photoionization line shapes, which do not depend on central-cell effects, are compared with calculations of the optical-absorption coefficient. In the [000]→[110] impurity cyclotron-resonance (ICR) transition nonparabolic effects are significant and have been included in the analysis.

The paper is organized as follows. In Sec. II the experimental aspects are presented. We present the experimental data and some of the results of the analysis in Sec. III. The details of the analysis are presented in Sec. IV. We discuss the relation of this work to the magnetic-field-induced metal-insulator transition in Sec. V. In Sec. VI we present our conclusions.

II. EXPERIMENTAL DETAILS

The far-infrared (FIR) magnetotransmission measurements have been carried out on bulk single-crystal sam-

TABLE I. Sample parameters

x	n (10^{14} cm^{-3})	μ (10^5 cm^2/V s)	m_0^* ($10^{-3}m_e$)	E_g (meV)	ϵ_0	c_j (10^{-17} meV cm^3)
0.270	1.0	0.80	12.5	200	16.1	2.33
0.237	0.6	1.96	8.53	125	16.3	2.37
0.224	0.6	1.20	6.82	100	16.2	3.02
0.204	0.3	2.70	5.01	67	16.0	2.77
0.198	2.1	4.50	4.00	56	16.4	3.23

ples of unintentionally doped n-type $Hg_{1-x}Cd_xTe$ grown by the quench-anneal process.[8] The relevant parameters for the samples used in this study are listed in Table I. Carrier densities and mobilities were deduced from low-field magnetotransport measurements at 77 K. In the handling and processing of the samples used in these studies, special precautions were taken because of the well-known problems with MCT. The samples for the FIR transmission measurements were first cleaved from the wafers with a sharp razor. To obtain an appropriate level of transmission, the sample thickness must be reduced to $\cong 25$ μm. They were first polished mechanically with alumina and then chemically polished to the desired thickness. Care in the etching process is important to minimize undesirable effects due to accumulation layers resulting from the surface potential of the oxide layer.[9] It is well known that this effect leads to both the shorting of the bulk by the surface conduction in transport measurements on low-density samples in high magnetic fields,[10] and to features in the transmission spectrum due to cyclotron resonance in the subbands of the accumulation layers and impurity transitions due to the surface-bound electrons, which may obscure the response of the bulk carriers. The samples were etched for 5 min in a 5% bromine-methanol solution and then stored in pure methanol solution to avoid exposure to air. They were then mounted on an undoped Ge substrate chosen because of the close match of its dielectric constant and thermal-expansion coefficient with MCT over a wide temperature range, thus minimizing effects of strain on the sample and interference fringes associated with the sample thickness. The Ge substrate was masked around the specimen with silver paint in order to prevent light leakage to the radiation detector.

The measurements were made in a cryostat in which the sample temperature could be varied from 1.5 to 100 K as measured with a calibrated carbon-glass resistor. The magnetic field from a 10-T superconducting solenoid was measured with a GaAs Hall probe. Magnetotransmission was studied using far-infrared radiation from an optically pumped cw laser in the spectral range $\lambda = 118.8$–888.9 μm. The Voigt-configuration cryostat was equipped with a linear polarizer, which could be rotated from outside the cryostat. In the Faraday-geometry cryostat a circular polarizer consisting of a linear polarizer and a set of crystal quartz $\lambda/4$ plates was placed ≈ 5 mm in front of the sample. The detector was a 4.2-K composite bolometer consisting of a small ($1\times1\times.075$ mm^3) doped Ge sensor epoxied to large-area ($10\times10\times.05$ mm^3) silicon wafer coated with an absorbing metal film.

III. RESULTS

Typical Voigt-geometry magnetotransmission spectra in $\mathbf{E}\|\mathbf{B}$ polarization are shown in Fig. 1 for the $x = 0.198$ sample for several photon energies. At 4.2 K two resonant features are seen in this sample. Similar spectra are observed in the $x = 0.204$ and 0.224 samples, while for the $x = 0.237$ and 0.270 samples only one absorption minimum was observed. In $\mathbf{E}\perp\mathbf{B}$ polarization neither of these resonances appear. Instead, the conduction-band cyclotron resonance is observed, but at much lower magnetic fields, or higher frequencies, as shown in Fig. 2 for the $x = 0.224$ sample. Important information for the identification of these resonances is provided by the temperature dependence of these spectra. The low-field resonance, which is clearly discernible in the Voigt geometry at 4.2 K (Fig. 3), is seen to weaken as the temperature is lowered to 1.5 K. This behavior is more pronounced for lower-x samples. The positions of these two resonances, together with the observed selection rules and temperature dependence, allow us to identify them as the impurity photoionization transition $[0\bar{1}0]\rightarrow[0\bar{1}k_z]$ (low field)

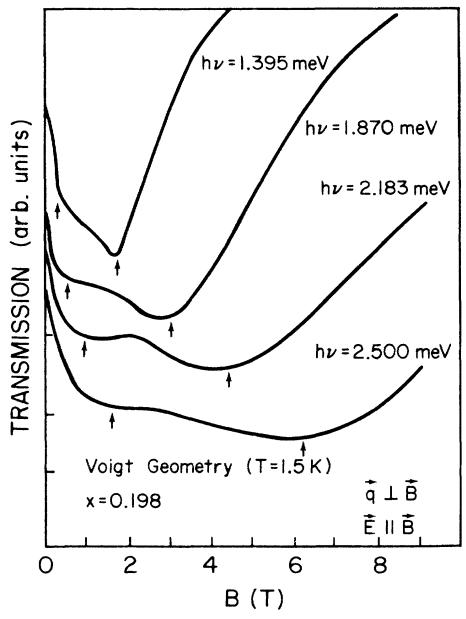

FIG. 1. Magnetotransmission spectra for the $x = 0.198$ sample in Voigt geometry in the $\mathbf{E}\|\mathbf{B}$ polarization at $T = 1.5$ K. The two resonances marked by arrows are identified as the $[0\bar{1}0]\rightarrow[0\bar{1}k_z]$ and $[000]\rightarrow[001]$ impurity transitions. The horizontal tic marks on the left-hand axis represent the zero-transmission levels for each successive trace.

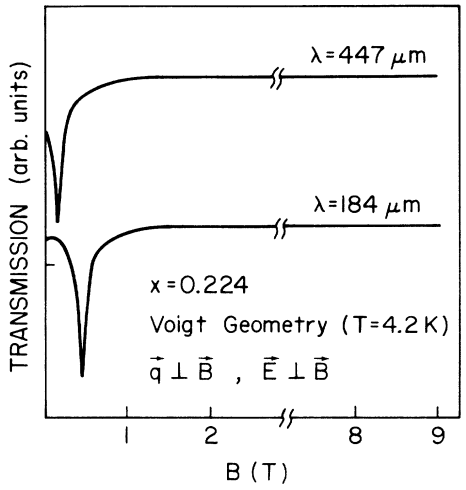

FIG. 2. Conduction-band cyclotron-resonance spectra for the $x=0.224$ sample in the **E⊥B**-polarization Voigt geometry. The tic mark on the left-hand axis indicates the zero-transmission level for the $\lambda=447$ μm line.

and the [000]→[001] donor transition (high field). The identification of the photoionization transition as $[0\bar{1}0]\rightarrow[0\bar{1}k_z]$ rather than $[000]\rightarrow[00k_z]$ follows from the temperature dependence. The weakening of the absorption at 1.5 K corresponds to the freeze-out of the electrons from the $[0\bar{1}0]$ level to the [000] ground state. The stronger temperature dependence for small x can be understood by noting that the separation between [000] and $[0\bar{1}0]$ energy levels decreases with x since the effective mass and, therefore, the effective Rydberg (Ry*) decreases with x. Calculations of the absorption strength, which will be presented in Sec. IV of this paper, indicate that the photoionization transition should be a factor of 10 weaker in the Faraday geometry (**E⊥B**) compared with the Voigt geometry (**E**‖**B**). This explains why the photoionization transition was not seen in the Faraday-geometry spectra.

The observed resonance energies are plotted against magnetic field in Figs. 4 and 5. The solid lines in the figures correspond to the calculated impurity transition energies of the [000]→[001] and $[0\bar{1}0]\rightarrow[0\bar{1}k_z]$ transitions based on the theory of hydrogenic donors in high magnetic fields. The details of the analysis are given in Sec. IV. The observed asymmetric broadening of the [000]→[001] resonance line shapes in these fixed frequency-field sweeping measurements can understood in terms of the effects of the nonlinear dependence of the transition energies with magnetic field. Since this dependence is sublinear, as seen in Fig. 4, the resonance linewidths increase as the photon energy increases and the low-field side of the absorption line tends to be sharper than the high-field side. This qualitative argument has been confirmed by comparisons of the magneto-transmission line shapes based on a Lorentz-oscillator model for the [000]→[001] transition and a calculation of the line shape of the $[0\bar{1}0]\rightarrow[0\bar{1}k_z]$ photoionization transition including lifetime broadening. The details of these calculations are given in Sec. IV. A result of a line-shape calculation, for the $x=0.198$ sample, is shown by the solid lines in Fig. 6. The fitting parameters $n(000)\simeq 7\times10^{13}$ cm^{-3}, $n(0\bar{1}0)\simeq 4\times10^{13}$ cm^{-3}, and the ac mobilities $\simeq 1.5\times10^5$ cm^2/V s and 2.5×10^5 cm^2/V s, respectively, are in satisfactory agreement with the values determined by transport measurements. In Fig. 7 we

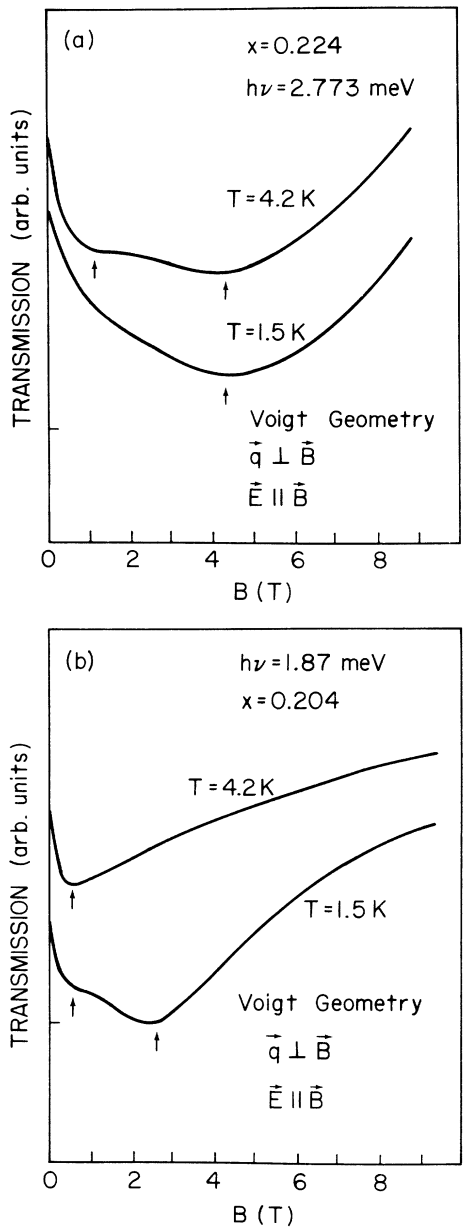

FIG. 3. Temperature dependence of the Voigt-geometry **E**‖**B** spectra showing the $[0\bar{1}0]\rightarrow[0\bar{1}k_z]$ and [000]→[001] transitions marked by arrows. The magnitude of the $[0\bar{1}0]\rightarrow[0\bar{1}k_z]$ absorption decreases at 1.5 K, while the [000]→[001] transition grows. (a) $x=0.224$ sample. (b) $x=0.198$ sample. A stronger temperature dependence is observed in the low-x sample. The tic mark on the left-hand axis indicates the zero-transmission level for $T=4.2$ K.

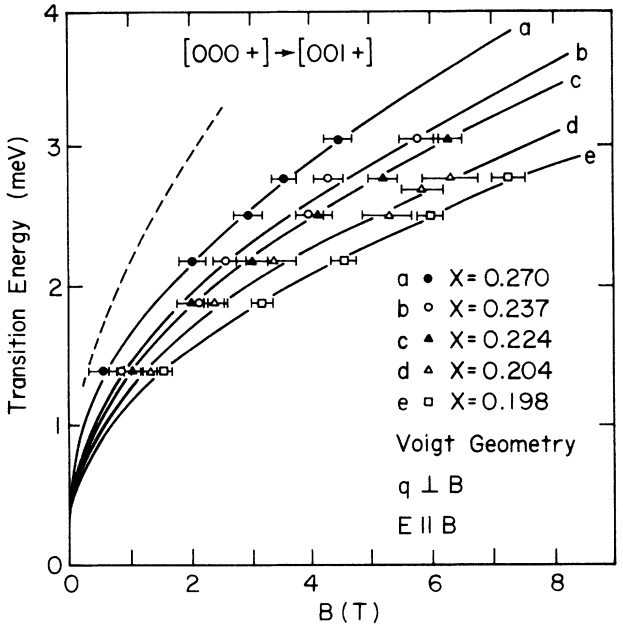

FIG. 4. Magnetic field dependence of the [000]→[001] impurity transition energy for samples with different x. The observed transition energies are indicated by data points with error bars. The solid lines correspond to the best fits including the central-cell effects with two parameters, ϵ_0 and C_j, whose values are listed in Table I for each sample. The fits are discussed in the text. The dashed curve represents the typical dispersion of the $[0\bar{1}0]\rightarrow[0\bar{1}k_z]$ photoionization transition, which is drawn in more detail in Fig. 5.

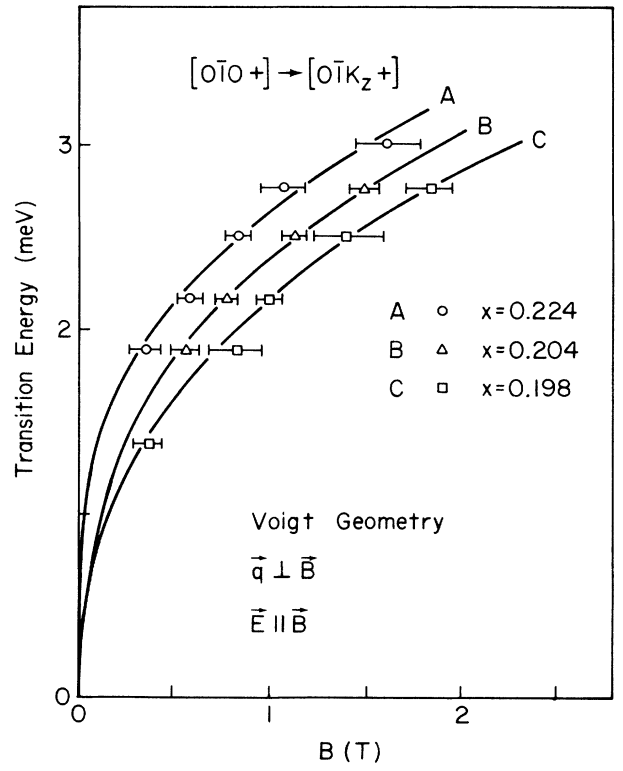

FIG. 5. Magnetic field dependence of the $[0\bar{1}0]\rightarrow[0\bar{1}k_z]$ photoionization transition energy. The solid lines are the calculated peak positions with the parameters given in the text.

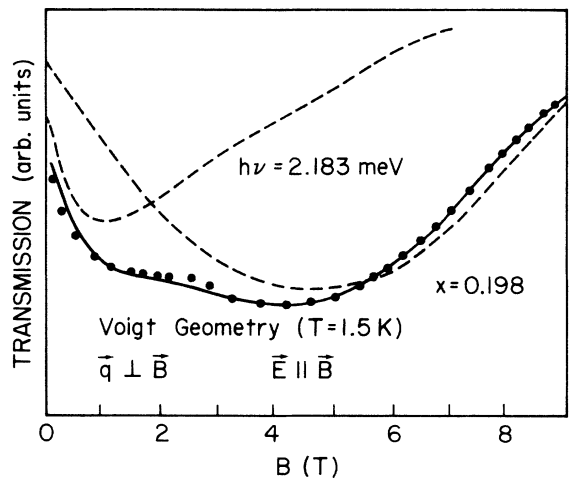

FIG. 6. Line-shape curve fit for the $x=0.198$ sample. The observed transmission is indicated by the solid circles. The solid line corresponds to the best fit to the calculations of the dielectric functions associated with the $[0\bar{1}0]\rightarrow[0\bar{1}k_z]$ and [000]→[001] transitions, each component of which is shown by the dashed lines.

show the line-shape fit for the $x=0.237$ sample where only the [000]→[001] transition was observed at 4.2 K. The good agreement of these fits shows that the asymmetric broadening of the [000]→[001] transitions is a natural consequence of laser magnetospectroscopy. It follows that narrower and more symmetric lines should be observed in broadband spectroscopy, in which the magnetic field is fixed and photon-energy scanned.

Typical results of magnetotransmission measurements in the Faraday geometry are shown in Fig. 8. This figure displays the temperature dependence of the relative strengths of two peaks which we identified as the

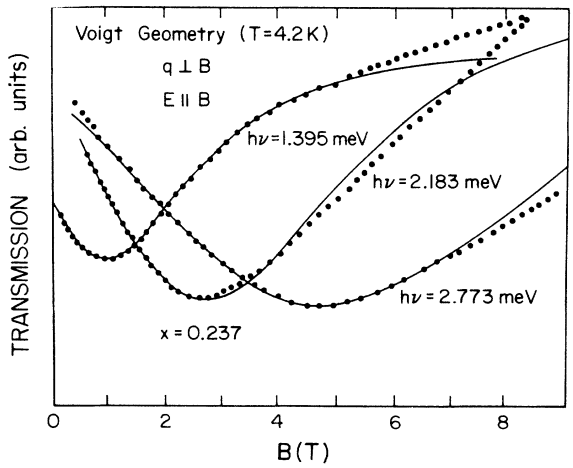

FIG. 7. Line-shape curve fits for the $x=0.237$ sample in which the only the [000]→[001] transition is observed. The solid curve is the fit to a Lorentz-oscillator-model dielectric function for each photon energy. From Ref. 6.

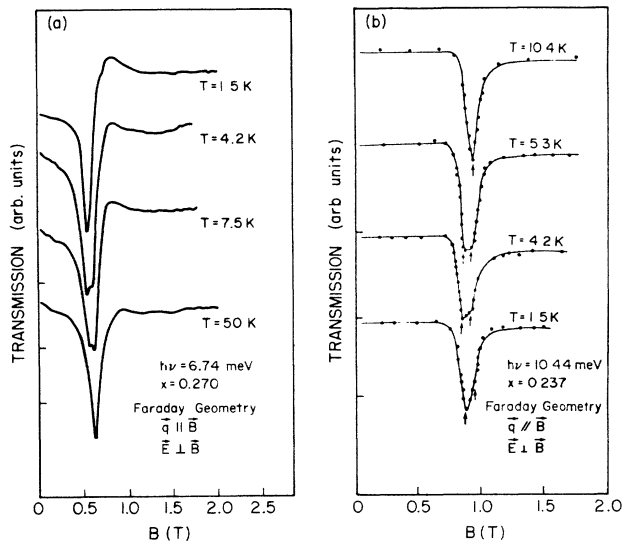

FIG. 8. (a) Temperature dependence of the Faraday-geometry magnetotransmission spectra for the $x=0.270$ sample at $\hbar\omega=6.78$ meV. The ICR absorption dominates over the CCR one at 1.5 K. The zero-transmission levels are shown by horizontal tic marks on the left-hand axis for each successive trace. (b) Temperature dependence of the Faraday-geometry magnetotransmission spectra for the $x=0.237$ sample at $\hbar\omega=10.44$ meV. The dots are the experimental data and the solid lines are the fits to a calculation based on a Lorentz-oscillator-model dielectric function for the impurity transition and a free-carrier dielectric function for the cyclotron resonance. The ICR and CCR positions are indicated by arrows. From Ref. 6.

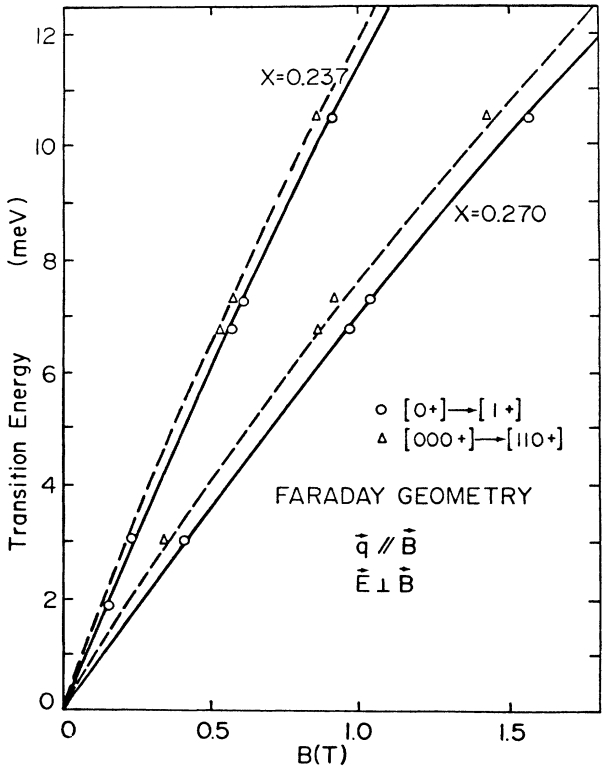

FIG. 9. Magnetic field dependence of the ICR and CCR for the Faraday geometry. The triangles and circles are the observed ICR and CCR, respectively, for the $x=0.237$ and 0.270 samples. The solid curves are the fits to the Bowers-Yafet nonparabolic $\mathbf{k}\cdot\mathbf{p}$ model for the CCR. The nonparabolic calculations for the ICR, described in the text, are given by the dashed lines. From Ref. 6.

conduction-band cyclotron resonance (CCR), [0+]→[1+], and the impurity cyclotron resonance (ICR), [000]→[110]. Both of these resonances were observed only in the electron-active mode of circularly polarized light. The solid lines in Fig. 8(b) are fits of these data to a model dielectric function consisting of a Lorentz-oscillator dielectric function for the ICR transition and a free-carrier dielectric function for the CCR. These fits yield the resonance positions, the linewidths, and the number density of carriers contributing to the two resonances. As the temperature is raised, the CCR transition grows at the expense of the ICR resonance. The sum of the two carrier densities is $\cong 7.5\times10^{13}$ cm^{-3}, compared to 6×10^{13} cm^{-3} as determined from 77-K magnetotransport. The linewidths interpreted as ac mobilities give $\mu_{CCR}\cong 2.4\times10^5$ cm^2/V s and $\mu_{ICR}\cong 1.4\times10^5$ cm^2/V s, compared to $\mu=2.0\times10^5$ cm^2/V s from 77-K transport. The agreement between the infrared and transport measurements is satisfactory considering the uncertainties in both. We note, however, that since the linewidths are comparable with the splittings, the CCR-ICR splittings cannot be measured with great precision for these samples. The dependence of the transition energies on magnetic field are shown in Fig. 9 for $x=0.237$ and 0.270. The solid curves along the cyclotron-resonance data are the best fits to the Bower-

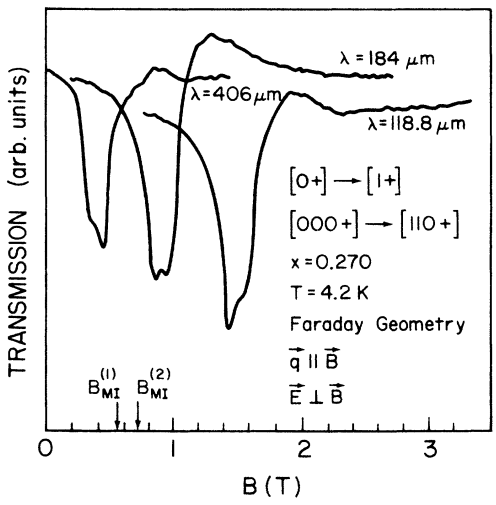

FIG. 10. Magnetic field dependence of the relative absorption strength of the ICR and CCR for the $x=0.270$ sample at $T=4.2$ K. The Mott critical fields corresponding to $\delta=0.25$ and 0.30 are indicated by arrows.

Yafet[11] nonparabolic $\mathbf{k}\cdot\mathbf{p}$ model for the conduction band. Simplified nonparabolic model calculations for the [000]→[110] impurity transition energies, which will be described in Sec. IV E, are given by the dashed lines. The magnetic field dependence of the relative absorption strength of the CCR and ICR at fixed temperature ($T=4.2$ K) is shown in Fig. 10 for the $x=0.270$ sample. The absorption strength of the ICR increases with magnetic field, because the binding energy of the donor ground state increases with field (magnetic freeze-out).

IV. ANALYSIS

A. General considerations

In the quantitative analysis of the experimental data with the theory of the hydrogenic donor in high magnetic fields, there are two important considerations. (1) The adiabatic approximation in which the motion of electrons along and perpendicular to the magnetic field is taken to be uncoupled and the transverse part of the wave function is approximated by the free Landau wave function. (2) The Γ_6 conduction band of MCT is strongly nonparabolic. MCT ($0.2<x<0.3$), like InSb, is a narrow-gap semiconductor with small effective masses in the conduction band ($m^*\cong 0.01$), so that the high-field-limit condition for the adiabatic approximation to be valid, $\gamma>10$ (where $\gamma=\hbar\omega_c/2\mathrm{Ry}^*$), can be achieved at modest magnetic fields; for example, $B>3.8$ kG for the $x=0.224$ sample. However, the nonparabolicity factor, $\hbar\omega_c/E_g$ (where E_g is the energy gap), generally is not small in MCT, and so band nonparabolicity can be important depending on the particular transitions involved. For the [000]→[001] intra-Landau-level impurity transition and the $[0\bar{1}0]\rightarrow[0\bar{1}k_z]$ photoionization transitions that are associated with the $N=0$ Landau level, the transition energies are relatively, small even at high fields. The highest photon energy we used for these transitions was $\simeq 3$ meV, so that $\hbar\omega/E_g\leq 0.06$ even for the smallest-gap sample ($x=0.198$, where $E_g=50$ meV). Therefore, for these transitions the parabolic effective-mass theory[12,13] is a good approximation. However, the effects of nonparabolicity cannot be neglected for the [000]→[110] (ICR) transitions where the transition energies are large at high fields.[14] The photon energies used in these measurements are as high as 10 meV, giving $\hbar\omega_c/E_g$ as large as 0.2. As we discuss in Sec. IV E, the nonparabolic behavior for this transition can be adequately accounted for by noting that, while the ground state [000] is weakly dependent on magnetic field, since it is associated with $N=0$ Landau level, the binding energy of the excited [110] state depends on the effective mass that is characteristic of the $N=1$ Landau level which increases with magnetic field.

In the parabolic formulation[12,13] of the hydrogenic donor theory the value of the impurity levels depends only on the dimensionless field parameter $\gamma=\frac{1}{2}\hbar\omega_c/(1\ \mathrm{Ry}^*)$. Consequently, the comparison of the data with the theoretical predictions can be made by scaling the published parabolic results with the values of m_0^* and ϵ_0 of our samples. Therefore it is very important to precisely determine the band-edge effective mass m_0^* and the static dielectric constant ϵ_0 for each sample. The considerations in the determination of these parameters for our samples is discussed in the next subsection.

B. Determination of m_0^* and $\mathbf{k}\cdot\mathbf{p}$ band parameters

To determine the band-edge effective mass m_0^* needed as an input parameter for calculations of resonance energies and line shapes, we have analyzed the Faraday-geometry cyclotron-resonance data. In treating the nonparabolicity of the Γ_6 conduction band, the Pidgeon-Brown model Hamiltonian,[15] which includes the far bands, provides the most complete account of the Landau levels in cubic narrow-gap semiconductors. However, the far bands are sufficiently far removed in energy from the Γ_8 band edge to give rise to only small contributions to the energy levels, in comparison to the strong $\mathbf{k}\cdot\mathbf{p}$ coupling between the closely spaced Γ_6, Γ_7, and Γ_8 bands. Therefore, we have used the simpler Bower-Yafet model,[11] which permits exact diagonalization of the Γ_6 conduction band, and Γ_7 and Γ_8 valence bands. This approach is quite adequate for the purposes of this paper, since we only need to determine the effective masses. According to the Bower-Yafet model, for $E\ll E_g+2\Delta/3$, the Landau levels in the conduction band at $k_z=0$ are given by

$$E(N,k_z,+)=-E_g+(E_g/2)\times[1+(4\hbar\omega_c/E_g)(N+\tfrac{1}{2}-u/2]^{1/2}\ , \tag{1}$$

where $u\equiv\frac{1}{2}[\Delta/(\Delta+3E_g/2)]$ and $\hbar\omega_c=eB/m_0^*c$.

The band-edge effective mass m_0^* is then

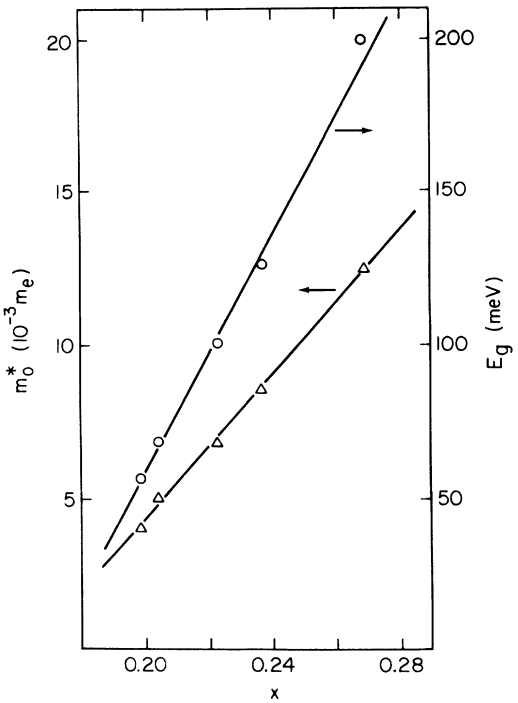

FIG. 11. x dependence of m_0^* and E_g at $T=4.2$ K as deduced from the cyclotron-resonance data.

$$m_0^* = (3\hbar^2/4P_0^2)[E_g(\Delta+E_g)/(\Delta+3E_g/2)] , \quad (2)$$

where P_0 is the $\mathbf{k}\cdot\mathbf{p}$ momentum matrix element and Δ the spin-orbit-coupling constant [taken as 960 meV (Ref. 16) for MCT]. From a least-squares fit of the cyclotron-resonance data, shown in Fig. 9, to Eq. (1), with m_0^* and E_g as fitting parameters, we obtained the values listed in Table I for our samples. In Fig. 11 we show the resulting x dependence of m_0^* and E_g for these samples. The energy gap so determined is found to be in satisfactory agreement with Hansen's recent empirical formula[17] for the dependence of E_g on Cd concentration x for MCT. From these results the corresponding value of the $\mathbf{k}\cdot\mathbf{p}$ momentum matrix element is $P_0 = -i\hbar\langle s|p_z|z\rangle/m_0 e = 8.67\times10^{-8}$ eV cm, which is close to the value $P_0 = 9.40\times10^{-8}$ eV cm in InSb.[18]

We have also considered polaron effects in the determination of m_0. Since the optical-phonon energies $\hbar\omega_0$ are relatively low in MCT ($\hbar\omega^{LO}\simeq 17$ meV and $\hbar\omega^{TO}\simeq 15$ meV),[19] the coupling with the optical phonons may also give rise to nonlinear dispersion of the cyclotron-resonance frequency with magnetic field. Since $\hbar\omega_c/E_g$ attains values as high as 0.2 in our MCT samples, the band nonparabolicity must be included in the analysis of the polaron effects. We adopt the analytical expression for the dispersion of the polaron energy given by Das Sarma and Mason.[20] In their treatment the nonparabolic energy levels are taken as the bare electron energies for a calculation of the self-energy corrections within the weak-coupling theory. Their result was further improved by Larsen,[21] who considered the nondiagonal band-mixing terms on the Fröhlich interaction neglected by Das Sarma and Mason. Larsen's resulting expression for the spin-up conduction band, at $k_z=0$, is given by

$$E(N,+) = X + Y\hbar\omega_c(N+\tfrac{1}{2}-u) \times[1-\hbar\omega_c(N+\tfrac{1}{2}-u)/YE_g^*] , \quad (3)$$

where $X = -\alpha\hbar\omega_0(1-\hbar\omega_0/2E_g)$, $Y = 1-\alpha/6(1+2.5\hbar\omega_0/E_g)$, and $E_g^{*-1} = E_g^{-1}+3\alpha/40\hbar\omega_0(1-31\hbar\omega_0/E_g)$. α is the Fröhlich constant. For $\hbar\omega_0/E_g \ll 1$, Eq. (3) reduces to the Bower-Yafet nonparabolic result. The analysis of the cyclotron-resonance data with Eq. (3) leads to values of m_0^* and E_g corrected for the polaron effect. For the sample with $x=0.237$, we find $m_0^* = (8.40\times10^{-3})m_0$, $E_g = 130$ meV, and $\alpha = 0.4970$. In comparison with the results in Table I, we see that the polaron effects give only a very small correction to the evaluation of the effective masses: $\Delta m_0^*/m_0^* \cong 1.4\%$. The range of photon energies used in these experiment is sufficiently below the optical-phonon energies and α is sufficiently small that the polaron effects are unimportant in our experiments.

The static dielectric constant ϵ_0, which is the other important parameter in parabolic donor theory, should also vary with x in MCT. Therefore, ϵ_0 also needs to be determined for each sample. For HgTe, $\epsilon_0\cong 20$ and, for $x=0.2$, different values for ϵ_0 have been reported in the literature,[19] $\epsilon_0\cong 17$ being representative. In the absence of consistent data for ϵ_0 in the literature, we have chosen to treat ϵ_0 as a fitting parameter in the analysis of the [000]→[001] impurity transitions. Therefore, these experiments provide a measure of ϵ_0 (the results are reported in Table I).

C. [000]→[001] transition and the central-cell effect

It was mentioned earlier that the nonparabolicity of the conduction band can be neglected in the [000]→[001] transition. The justification for this conclusion is that calculations show that nonparabolic corrections to the initial ([000]) and final state ([001]) nearly cancel in the field range of our measurements ($B \le 9$ T), so that the predictions of parabolic theory are quite accurate.[22] There is, however, a significant correction to the resonance energy due to chemical shifts of the [000]-state energy of the donor arising from the interaction of the bound electron with its ion core. This "central-cell effect" can lead to impurity-specific shifts of the resonances in which the initial state is the ground state.[23–25] The resolution of distinct donor transitions from the residual unintentional impurities can be used, in principle, to identify these impurities and could lead to their elimination and the development of higher-purity MCT. In the materials currently available, however, the large impurity-induced linewidths preclude resolving the central-cell splittings from different donor species.

The central-cell correction to the jth donor may be expressed as[26]

$$\Delta E = C_j|\Psi(0)|^2 , \quad (4)$$

where $\Psi(0)$ is the envelope wave function evaluated at the origin and C_j is a magnetic-field-independent constant for the jth donor, which depends on the symmetry of Luttinger-Kohn basis functions at the Γ point. We adopt the trial wave functions of Yafet, Keys, and Adams[12] (YKA) for the ground state, [000], in the high-field limit, which is given by[12]

$$\Psi(r) = (2^{3/2}a_\perp^2 a_\parallel \pi)^{-1/2} \times \exp[-(x^2+y^2)/4a_\perp^2 - z^2/4a_\parallel^2] , \quad (5)$$

where $a_\perp$ and $a_\parallel$ are the field-dependent variational parameters in units of the zero-magnetic-field effective Bohr radius a_0^*. The [000]→[001] resulting transition energy, in units of Ry*, is given by

$$E = E_0(\gamma) + C_j[a_\perp^2(\gamma)a_\parallel(\gamma)]^{-1} , \quad (6)$$

where E_0 is the [000]→[001] transition energy calculated within the parabolic theory, without the central-cell correction. Note that the transition energy depends on the magentic field m_0^* and on ϵ_0 through the dimensionless field parameter γ and the Ry* energy unit. In the data analysis, therefore, we fit our data to Eq. (6) for the transition energy with C (neglecting, possibly, different donor species) and ϵ_0 as two fitting parameters. For E_0 we use Larsen's parabolic results.[22] The resulting fits are shown in Fig. 6 as solid lines for each sample, and the corresponding parameters are summarized in Table I.

The values for ϵ_0 are close to the values in the literature for MCT, and the magnitude and sign of the central-cell correction is reasonable in comparison with InSb results.[27] Because of the large linewidths in these MCT resonances, however, the resulting parameter values should be considered only as estimations.

D. The $[0\bar{1}0]\rightarrow[0\bar{1}k_z]$ photoionization transition

The qualitative characteristics of the photoionization transitions were discussed in Sec. III. In this subsection we present the line-shape calculations needed to verify our identifications. Theoretical calculations for the energy levels of isolated donors as a function of magnetic field have been reported by many authors[13,14] since the pioneering work of YKA.[12] For the case of the photoionization transition, however, the experimentally observed resonance position is not simply the difference between the discrete level and the bottom of a Landau continuum. The k_z dependence of the dipole matrix elements and carrier-lifetime broadening both influence the position of the absorption peak. Therefore, to analyze the photoionization transitions it is necessary to calculate the optical-absorption coefficient including the line broadening. The only published work to date is that of Wallis and Bowlden[13] for the $[000]\rightarrow[00k_z]$ transition for the case $\gamma=35$. Also, the broadening parameter they used, to represent InSb data, is much too small for our MCT samples. These results are clearly insufficient for the analysis of our data. Therefore, here we present a full calculation for the photoionization absorption for both the Voigt and Faraday geometries.

Since these transitions are all within the lowest Landau level and $\hbar\omega \ll E_g$, it is sufficient to use parabolic theory. The wave function for the continuum state is given by[28]

$$\Psi_{lm}(r)=\Phi_{lm}(\sigma,\phi)\exp(ik_z z) , \tag{7}$$

where $\Phi_{lm}(\sigma,\phi)=c_0(l,m)e^{im\phi}\sigma^{m/2}e^{-\sigma/2}L_l^m(\sigma)$, with $[c_0(l,m)]^2=(\gamma/2\pi L_z)\,l!/[(l+m)!]^3$, $\sigma=\gamma\rho^2/2$, and $L_{l+m}^m(\sigma)$ is the associated Laguerre polynomial given by

$$L_{l+k}^k(\sigma)=(-1)^k\Gamma(k+l+1)\times\sum_{p=0}^{l}(-1)^{l-p}{}_{k+l}C_p\,\sigma^{l-p}/(l-p)!$$

For the bound-state wave function we use the one-parameter Wallis-Bowlden trial function[13] given by

$$\Psi_{lm\lambda}(r)=\Phi_{lm}(\sigma,\phi)P_\lambda(z)\exp(-\gamma\beta^2z^2/4) , \tag{8}$$

where $P_\lambda(z)$ represents a set of orthogonal polynomials and β is the variational parameter which is a different function of γ for each $(lm\lambda)$ state. Calculating the transition matrix elements and using standard second-order perturbation theory with a Lorentzian line-shape function with a line-broadening parameter $\hbar\Gamma$, the optical-absorption coefficient $\alpha(E)$ for the Voigt-geometry ($\mathbf{E}\|\mathbf{B}$) transitions $[000]\rightarrow[00k_z]$ and $[0\bar{1}0]\rightarrow[0\bar{1}k_z]$ are

$$\alpha_{lm\lambda}(E)=[4ne^2(2\pi)^{5/2}/\pi^2\epsilon_0^{1/2}\hbar c]\gamma^{-5/2}\beta_{lm\lambda}^{-5}\Pi(E) , \tag{9}$$

where

$$\Pi(E)=\int_{-\infty}^{\infty}dk_z(\gamma+k_z^2-E_{lm\lambda})k_z^2\exp(-2k_z^2/\gamma\beta_{lm\lambda}^2)\times\{\Gamma/[(\gamma+k_z^2-E_{lm\lambda}-E)^2+\Gamma^2]\} ,$$

and those for the Faraday-geometry transitions $[000]\rightarrow[0\bar{1}k_z]$ and $[0\bar{1}0]\rightarrow[00k_z]$ are

$$\alpha_{lm\lambda}(E)=[8ne^2(2\pi)^{1/2}/\epsilon_0^{1/2}\hbar c]\gamma^{-3/2}\beta_{lm\lambda}^{-1}\Pi(E) , \tag{10}$$

where

$$\Pi(E)=\int_{-\infty}^{\infty}dk_z(\gamma+k_z^2-E_{lm\lambda})\exp(-2k_z^2/\gamma\beta_{lm\lambda}^2)\times\{\Gamma/[(\gamma+k_z^2-E_{lm\lambda}-E)^2+\Gamma^2]\} .$$

For the values of the donor energy $E_{lm\lambda}(\gamma)$ and the variational parameter $\beta_{lm\lambda}(\gamma)$, we use the analytical results of Wallis and Bowlden,[13] which are smooth functions of γ only. The examples of line shapes calculated from these results are plotted in Fig. 12. For the case of the broadening parameter $\hbar\Gamma=0.2$ Ry*, the absorption in Faraday geometry is seen to be much sharper than that

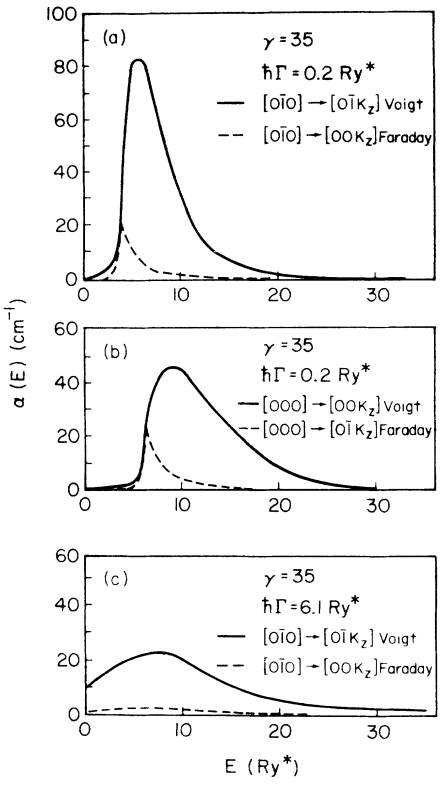

FIG. 12. Calculated photoionization absorption spectra. (a) $\gamma=35$ and $\hbar\Gamma=0.2$ Ry*; solid line, $[0\bar{1}0]\rightarrow[0\bar{1}k_z]$ transition in the Voigt geometry; dashed line, $[0\bar{1}0]\rightarrow[00kz]$ transition in the Faraday geometry. (b) $\gamma=35$ and $\hbar\Gamma=0.2$ Ry*: solid line, $[000]\rightarrow[00k_z]$ transition in the Voigt geometry; dashed line, $[000]\rightarrow[0\bar{1}k_z]$ transition in the Faraday geometry. (c) $\gamma=35$ and $\hbar\Gamma=6.1$ Ry*: solid line, $[0\bar{1}0]\rightarrow[0\bar{1}kz]$ transition in the Voigt geometry; dashed line, $[0\bar{1}0]\rightarrow[00k_z]$ transition in the Faraday geometry.

in Voigt geometry. However, the integrated strength of the Faraday-geometry absorption is much smaller than the Voigt case. Also, we see that the $[0\bar{1}0]\rightarrow[0\bar{1}k_z]$ transition is stronger than the $[000]\rightarrow[00k_z]$ transition. This can be understood in terms of the corresponding dipole matrix elements. The transition matrix element for the optical-absorption coefficient has the form $\int d^3r\,\Psi_i^*(r)z\Psi_j(r)$ in Voigt geometry, where the i (j) are the initial (final) states. Since the wave function for the $[0\bar{1}0]$ state has a node at the origin and for the [000] state an antinode, a larger value of the matrix element results for the $[0\bar{1}0]\rightarrow[0\bar{1}k_z]$ transition. The strength and position of the absorption peak depends strongly on the value of broadening parameter $\hbar\Gamma$. As $\hbar\Gamma$ increases, the spectra broaden and the peak position shifts to higher energy. For broadening suitable for the measurements reported here, $\hbar\Gamma\cong 5$ Ry*, the Faraday-geometry absorption is found to be very weak. Therefore, the determination of the value of Γ is very important in the comparison of the experimental data with calculated line shapes.

We have attempted to fit the measured transmission data to calculated line shapes. Since both $[000]\rightarrow[001]$ and $[0\bar{1}0]\rightarrow[0\bar{1}k_z]$ transitions contribute the absorption spectra, we use Eq. (9) for the absorption coefficient, α_1, for the photoionization $[0\bar{1}0]\rightarrow[0\bar{1}k_z]$ transition and a Lorentzian line shape for the absorption coefficient, α_2, for the $[000]\rightarrow[001]$ transition. The transmission is calculated from

$$T=2(1-R)e^{-\alpha d}\ , \tag{11}$$

where R is the reflectance, d is the sample thickness, and $\alpha=\alpha_1+\alpha_2$. The fitting parameters are the relative carrier densities and broadening constants. The resulting fits are shown by the solid lines in Fig. 6. The value for $\hbar\Gamma$ in the fit was $\cong 6.1$ Ry*, which corresponds to an ac mobility of about 1.5×10^5 cm^2/V s. This mobility value is satisfyingly close to the values deduced from transport measurements. Figure 12(c) shows the photoionization spectra for $\hbar\Gamma=6.1$ Ry* in the Voigt and Faraday geometry, respectively. It is seen that the calculated absorption coefficient in Faraday geometry becomes flat and nearly imperceptible in comparison with the Voigt-geometry case. This result explains the absence of photoionization absorption in the Faraday configuration, even though the transitions satisfy the $\Delta m=\pm1$ selection rule.

We have calculated $\alpha(\gamma)$ for the $[0\bar{1}0]\rightarrow[0\bar{1}k_z]$ transition with the fitting parameters $\hbar\Gamma=7.6$, 6.1, and 6.1 Ry* for the $x=0.224$, 0.204, and 0.198 samples, and determine the maximum absorption positions $\gamma_{\max}$ for each fixed measurement photon energy E and each sample. Typical spectra, $\alpha(\gamma)$, are shown for several photon energies for the $x=0.198$ sample in Fig. 13. The resonance positions $\gamma_{\max}$ are converted to the resonance magnetic fields by using m_0^* and ϵ_0 of each sample. The resulting resonance fields are plotted as solid lines in Fig. 5 for each sample. The overall agreement for all the samples with the observed resonant fields are seen to be quite good. We take this agreement to be strong evidence for this identification of the experimental data with the $[0\bar{1}0]\rightarrow[0\bar{1}k_z]$ photoionization transition. This conclusion is further strengthened by the observed weakening of the resonance as the sample temperature is lowered and the electrons freeze out onto the [000] level.

E. [000]→[110] transition: Impurity cyclotron resonance

The band nonparabolicity can not be neglected in the analysis of the $[000]\rightarrow[110]$ inter-Landau-level impurity transitions since $\hbar\omega/E_g$ is not small in the measurements. Because the binding energies in nonparabolic theory are no longer functions only of the dimensionless field parameter γ, we can not simply scale the published nonparabolic results by using suitable m_0^* and ϵ_0. Instead, we must perform a nonparabolic calculation of the energy levels. Fortunately, a simple approximate calculation is found to be adequate for the conditions of our experiments. We start with the exact Hamiltonian in Luttinger-Kohn effective-mass theory,[29] which is given by

$$H_{nn'}=H^0_{nn'}+V(r)\delta_{nn'}\ , \tag{12}$$

where $H^0_{nn'}$ is the free-carrier–nonparabolic-multiband Hamiltonian, $V(r)$ is the impurity potential, and n,n' are band indices. In the strong-field limit $V(r)$ can be treated as a small perturbation to $H^0_{nn'}$. We can therefore exploit the fact that the results of parabolic theory can be scaled with only two parameters, namely m_0^* and ϵ_0. The scheme for calculation consists of two steps. (1) From $H^0_{nn'}$ we derive an effective mass $m^*(B,N,s)$ which is a function of magnetic field B, Landau level N, and spin s. (2) We then scale the parabolic binding energy of each impurity level belonging to same N,s quantum numbers using $m^*(B,N,s)$. Mathematically, this procedure is equivalent to the diagonalization of $H_{nn'}$, neglecting the diagonal Coulomb potential term first and then treating it as a perturbation, which should be rigorous to leading order in $V(r)$. For $H^0_{nn'}$, we adopt the Bower-Yafet model Hamiltonian,[11] which is an 8×8 matrix, because it treats the Γ_6 conduction band and Γ_7 and Γ_8 valence bands only. The more exact Pidgeon-Brown Hamiltonian,[15] which includes the coupling among other levels beyond the Γ_6, Γ_8, and Γ_7 bands, in second-order perturbation theory, is inconvenient in our calculation scheme since it does not lead to an analytic expression for $m^*(B,N,s)$. Moreover, the added sophistication is not warranted for the relatively broad donor resonances in MCT. Using the symmetric gauge for the vector potential and assuming $E\ll E_g+2\Delta/3$, the effective mass at $k_z=0$ is given by

$$m^*(B,N,+)=m_0^*\{1+4\hbar eB/m_0^*cE_g[N+\tfrac{1}{2}+(\Delta/4\Delta+6E_g)]\}^{1/2}\ . \tag{13}$$

We use the parameters resulting from the cyclotron-resonance analysis listed in Table I for the value of the zero-field conduction-band-edge effective mass m_0^* and energy gap E_g. For each level we then calculate $\gamma(B,N,+)$ using $m^*(B,N,+)$, and then use the parabolic theory to estimate the binding energy (relative to the Landau level) using $\gamma(B,N,+)$ in place of γ. This procedure should be valid as long as the binding energies are

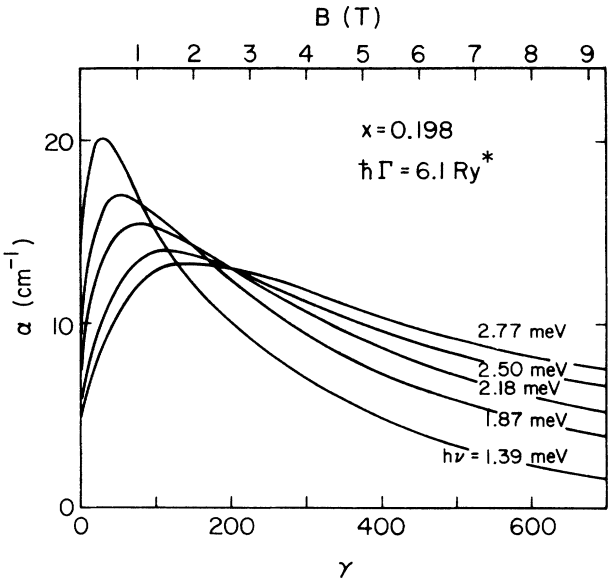

FIG. 13. $[0\bar{1}0]\rightarrow[0\bar{1}k_z]$ photoionization absorption spectrum vs field parameter γ for different fixed photon energies for the $x=0.198$ sample. The chosen broadening parameter $\hbar\Gamma=6.1$ Ry* is the value corresponding to the best fit of the transmission spectra.

small compared to E_g, as we find in these experiments. For the binding energies of the impurity levels within the parabolic theory, we use the calculations of Larsen.[14] The results of the analysis are shown as dotted lines in Fig. 9. Since the initial state of this transition is the ground state, [000], we have also included the central-cell correction discussed in Sec. IV C. The agreement between experimental data and the predicted dispersion is seen to be quite satisfactory.

V. MAGNETIC-FIELD-INDUCED METAL-INSULATOR TRANSITION

The magnetic field dependence of the relative absorption strength of the ICR and CCR at fixed temperature ($T=4.2$ K) for the $x=0.270$ sample is shown in Fig. 10. Since the binding energy of the donor [000] ground state increases with magnetic field, at finite temperature the magnitude of the ICR absorption should increase relative to the CCR as the magnetic field increases. This is the magnetic freeze-out effect. The dominance of the CCR over the ICR at the resonant field of 4 kG for $\lambda=406$ μm is due to thermal excitation of the electrons from the impurity band to the conduction band. At sufficiently low temperature, most of electrons should condense onto the donor sites, and only the ICR will be observed. It is very interesting to note that the ICR is observed even below the critical field $B_{M\text{-}I}$ for the magnetic-field-induced metal-insulator transition. For the low-carrier-density samples used in our optical measurements, the determination of the critical field by transport measurement has been found to be difficult because of the shorting of the bulk conduction by the surface. Instead, we estimate $B_{M\text{-}I}$ from the Mott criterion $[n^{1/3}a^*(B)=\delta)$, where the effective Bohr radius is $a^*(B)=(a_\perp^2 a_\parallel)^{1/3}$. The parameters $a_\perp$ and $a_\parallel$ as a function of magnetic field are those given by YKA.[12] The experimental value of δ has been found to be 0.25–0.26 for many systems of doped semiconductors over a large range of carrier densities.[30,31] However, the most recent data for the magnetic-field-induced metal-insulator transition in MCT ($x=0.21$) obtained by Shayegan *et al.* indicate $\delta\cong 0.3$.[32] Therefore, for the $x=0.270$ sample, $B_{M\text{-}I}$ from the Mott condition would be 7.0 and 5.8 kG for $\delta=0.25$ and 0.3, respectively.

The persistence of the ICR below the critical field for the metal-insulator transition has also been recently observed in the wide-gap semiconductor GaAs.[33] These observations suggest that the magnetic-field-induced metal-insulator transition in these materials takes place within the donor impurity band, which is well separated from the conduction band. Additional evidence for this conclusion has been found from the analysis of the Hall effect near the metal-insulator transition in MCT.

VI. CONCLUSIONS

We have observed the Voigt-geometry impurity transitions $[000]\rightarrow[001]$ and $[0\bar{1}0]\rightarrow[0\bar{1}k_z]$ and the Faraday-geometry $[000]\rightarrow[110]$ transition in $Hg_{1-x}Cd_xTe$. All of the observations are completely consistent with the properties of the hydrogenic donor in high magnetic fields. The central-cell correction and nonparabolicity are found to be important factors in the analysis. However, the large linewidth observed in the $[000]\rightarrow[001]$ transition precludes observing the fine structures due to the chemical shifts of individual donors for the samples currently available. To resolve these shifts, measurements on higher-mobility samples using broadband spectroscopy may be required. Observations of these different impurity transitions in both Voigt and Faraday configurations and their consistency with the theory permit us to conclude that the narrow-gap semiconductor n-type $Hg_{1-x}Cd_xTe$ ($0.2\leq x\leq 0.3$) has the same low-temperature, high-magnetic-field electronic behavior as n-type InSb: i.e., magnetic-field-induced localization of the Mott-Anderson type with the condensation of the electrons onto donor sites. These results disprove the claims of a Wigner-crystal ground state for this system.[2,4]

ACKNOWLEDGMENTS

We thank D. A. Nelson for the samples. Also, we are grateful for useful discussions with M. Shayegan and V. J. Goldman. This work was supported in part by the U.S. Office of Naval Research under Grant No. N00014-89-5-1551 and by the U.S. National Science Foundation under Grant No. DMR-87-05002.

[1]J. Durkan, R. J. Elliot, and N. H. March, Rev. Mod. Phys. **40**, 812 (1968); R. Mansfield, M. Abdul-Gader, and P. Fozooni, in *Proceedings of the International Conference on Heavy Doping and the Metal-Insulator Transition in Semiconductors, Santa Cruz (1984),* edited by P. Landsberg [Solid-State Electron. **28**, 109 (1985)].

[2]G. Nimtz, F. B. Schlicht, E. Tyssen, R. Dornhaus, and L. D. Haas, Solid State Commun. **32**, 669 (1979).

[3]M. Shayegan, V. J. Goldman, and H. D. Drew, Phys. Rev. B **38**, 5585 (1988).

[4]T. F. Rosenbaum, S. B. Field, D. A. Nelson, and P. B. Littlewood, Phys. Rev. Lett. **54**, 241 (1985); S. B. Field, D. H. Reich, T. F. Rosenbaum, P. B. Littlewood, and D. A. Nelson, Phys. Rev. B **38**, 1856 (1989).

[5]V. J. Goldman, H. D. Drew, M. Shayegan, and D. A. Nelson, Phys. Rev. Lett. **56**, 968 (1986).

[6]J. B. Choi, L. S. Kim, H. D. Drew, and D. A. Nelson, Solid State Commun. **65**, 547 (1988).

[7]J. M. Perez, J. E. Furneaux, and R. J. Wagner, J. Vac. Soc. Technol. A **6**, 2681 (1988).

[8]D. A. Nelson, W. M. Higgins, and R. A. Lancaster, Proc. SPIE **227**, 48 (1980).

[9]W. Zhao, C. Mazure, F. Koch, J. Ziegler, and H. Maier, Surf. Sci. **142**, 400 (1984); J. B. Mullin and A. Royle, J. Phys. D **17**, L69 (1984).

[10]J. P. Stadler, G. Nimtz, B. Schlicht, and G. Remenyi, Solid State Commun. **52**, 67 (1984).

[11]R. Bowers and Y. Yafet, Phys. Rev. **115**, 1165 (1959).

[12]Y. Yafet, R. W. Keys, and E. N. Adams, J. Phys. Chem. Solids **1**, 137 (1956).

[13]R. F. Wallis and H. J. Bowlden, J. Phys. Chem. Solids **7**, 78 (1958).

[14]D. M. Larsen, J. Phys. Chem. Solids **29**, 271 (1968); W. Trzeciakowski, M. Baj, S. Huant, and L.-C. Brunel, Phys. Rev. B **33**, 6846 (1986).

[15]C. R. Pidgeon and R. N. Brown, Phys. Rev. **146**, B575 (1966); M. H. Weiler, in *Semiconductors and Semimetals,* edited by R. K. Beer and A. C. Willardson (Academic, New York, 1981), Vol. 16, p. 119.

[16]M. A. Kinch and D. D. Buss, in *The Physics of Semimetals and Narrow-Gap Semiconductors, Dallas (1970),* edited by D. L. Carter and R. T. Bates (Pergamon, Oxford, 1971); H. Kahlerand, G. Bauer, Phys. Rev. Lett. **30**, 1211 (1973); B. D. McCombe, R. G. Wagner, and G. A. Prinz, *ibid.* **25**, 87 (1970).

[17]G. L. Hansen, J. L. Schmit, and T. N. Casselman, J. Appl. Phys. **53**, 7099 (1982).

[18]M. W. Goodwin and D. G. Seiler, Phys. Rev. B **27**, 3451 (1983).

[19]D. L. Carter, M. A. Kinch, and D. D. Buss, in *The Physics of Semimetals and Narrow-Gap Semiconductors, Dallas (1970),* edited by D. L. Carter and R. T. Bates (Pergamon, Oxford, 1971); J. Baars and F. Sorger, Solid State Commun. **10**, 875 (1972).

[20]S. Das Sarma and B. A. Mason, Phys. Rev. B **31**, 1177 (1985).

[21]D. M. Larsen, Phys. Rev. B **34**, 5927 (1986).

[22]D. M. Larsen (private communication).

[23]R. Kaplan, R. A. Cooke, R. A. Stradling, and F. Kuchar, in *The Application of High Magnetic Fields in Semiconductor Physics,* edited by J. F. Ryan (Clarendon, Oxford, 1978), p. 397.

[24]F. Kuchar, R. Kaplan, R. J. Wagner, R. A. Cooke, R. A. Stradling, and P. Vogl, J. Phys. C **17**, 6415 (1984).

[25]C. J. Armistead, P. Knowles, S. P. Najda, and R. A. Stradling, J. Phys. C **17**, 6415 (1984).

[26]H. R. Fetterman, D. M. Larsen, G. E. Stillman, P. E. Tannenwald, and J. Waldman, Phys. Rev. Lett. **26**, 975 (1971).

[27]R. Kaplan, Phys. Rev. **181**, 1154 (1969).

[28]R. B. Dingle, Proc. R. Soc. London, Ser. A **211**, 500 (1952).

[29]J. M. Luttinger and W. Kohn, Phys. Rev. **97**, 869 (1955).

[30]S. Ishida and E. Otsuka, J. Phys. Soc. Jpn. **43**, 124 (1974); M. Pepper, J. Non-Cryst. Solids **32**, 161 (1979).

[31]T. F. Rosenbaum, R. F. Milligan, M. A. Paalanen, G. A. Thomas, and R. H. Bhatt, Phys. Rev. B **27**, 7509 (1983).

[32]M. Shayegan, H. D. Drew, D. A. Nelson, and P. M. Tedrow, Phys. Rev. B **31**, 6123 (1985).

[33]M.-W. Lee, D. Romero, H. D. Drew, M. Shayegan, and B. S. Elman, Solid State Commun. **66**, 23 (1988).